molecular pharmaceutics

pubs.acs.org/molecularpharmaceutics

Article

Modulation of the Pharmacokinetics of a Radioligand Targeting Carbonic Anhydrase-IX with Albumin-Binding Moieties

Shimpei Iikuni,*,§ Yuya Okada,§ Yoichi Shimizu, Hiroyuki Watanabe, and Masahiro Ono*

Cite This: https://dx.doi.org/10.1021/acs.molpharmaceut.0c00953

Read Online

ACCESS | Metrics & More | Article Recommendations | Supporting Information

ABSTRACT: The expression of carbonic anhydrase-IX (CA-IX) in tumors can lead to a poor prognosis; thus, CA-IX has attracted much attention as a target molecule for cancer diagnosis and treatment. An ^{111}In-labeled imidazothiadiazole sulfonamide (IS) derivative, [^{111}In]In-DO3A-IS1, exhibited marked tumor accumulation but also marked renal accumulation, raising concerns about it producing a low signal/background ratio and a high radiation burden on the kidneys. In this study, four ^{111}In-labeled IS derivatives, IS-[^{111}In]In-DO2A-ALB1−4, which contained four different kinds of albumin binder (ALB) moieties, were designed and synthesized with the aim of improving the pharmacokinetics of [^{111}In]In-DO3A-IS1. Their utility for imaging tumors that strongly express CA-IX was evaluated in mice. An *in vitro* binding assay of cells that strongly expressed CA-IX (HT-29 cells) was performed using acetazolamide as a competitor against CA-IX, and IS-[^{111}In]In-DO2A-ALB1−4 did not exhibit reduced binding to HT-29 cells compared with [^{111}In]In-DO3A-IS1. In contrast, IS-[^{111}In]In-DO2A-ALB1−4 showed a greater ability to bind to human serum albumin than [^{111}In]In-DO3A-IS1 *in vitro*. In an *in vivo* biodistribution study, the introduction of an ALB moiety into the ^{111}In-labeled IS derivative markedly decreased renal accumulation and increased HT-29 tumor accumulation and blood retention. The pharmacokinetics of the IS derivatives varied depending on the substituted group within the ALB moiety. Single-photon emission computed tomography imaging with IS-[^{111}In]In-DO2A-ALB1, which showed the highest tumor/kidney ratio in the biodistribution study, facilitated clear HT-29 tumor imaging, and no strong signals were observed in the normal organs. These results indicate that IS-[^{111}In]In-DO2A-ALB1 may be an effective CA-IX imaging probe and that the introduction of ALB moieties may improve the pharmacokinetics of CA-IX ligands.

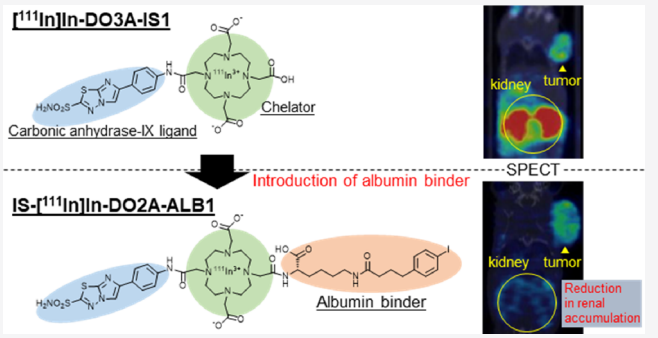

KEYWORDS: *carbonic anhydrase-IX, imidazothiadiazole sulfonamide, albumin binder, pharmacokinetics, radiometallic chelate*

INTRODUCTION

In mammals, the α-family of carbonic anhydrase (CA) has been reported to contain 16 members, which are closely related zinc metalloenzymes.[1] Each isozyme exhibits different catalytic activity, subcellular localization, and tissue distribution characteristics. CA-IX plays a key role in regulating intra- and extracellular pH, as it catalyzes the reversible hydration of carbon dioxide to a bicarbonate anion and proton and promotes cancer cell survival.[1−4] In addition, CA-IX contributes to tumor invasion and metastasis.[5] The expression of CA-IX is markedly increased in many types of tumors through hypoxia-inducible factor-1.[1] CA-IX expression is upregulated not only by hypoxia but also by a deficit of the von Hippel Lindau tumor suppressor protein, which is generally found in patients with clear cell renal cell carcinoma.[6−10] On the other hand, CA-IX is not expressed in normal tissues except in the gastrointestinal tract.[11] In addition, CA-IX is located at the cell surface; therefore, it is considered to be a promising endogenous target for the diagnostic imaging of cancer.

To date, many CA-IX imaging probes based on antibodies or small-molecule CA-IX inhibitors have been reported.[12−15] We previously reported an ^{111}In-labeled CA-IX imaging probe, [^{111}In]In-DO3A-IS1, which was based on our original CA-IX ligand, imidazothiadiazole sulfonamide (IS) (Figure 1).[16] [^{111}In]In-DO3A-IS1 demonstrated a greater uptake (8.71% injected activity/g at 24 h postinjection) by tumors that strongly expressed CA-IX (HT-29 tumors) than previously reported probes,[17−21] and HT-29 tumors were clearly visualized in model mice that had been injected with the probe on single-photon emission computed tomography (SPECT). However, [^{111}In]In-DO3A-IS1 exhibited marked renal accumulation (65.1−115% injected activity/g at 1−24 h

Received: September 23, 2020
Revised: January 6, 2021
Accepted: January 8, 2021

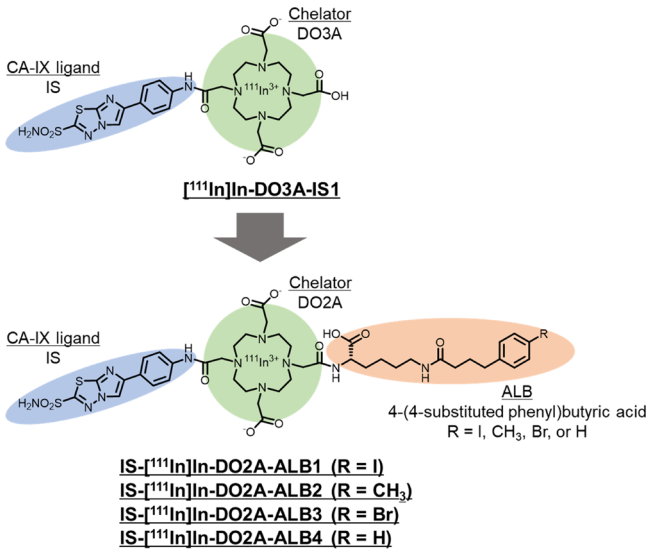

Figure 1. Chemical structures of IS-[^{111}In]In-DO2A-ALB1−4 and [^{111}In]In-DO3A-IS1. An albumin binder (ALB) was introduced into an imidazothiadiazole sulfonamide (IS) derivative to improve its pharmacokinetics.

postinjection). Most CA-IX imaging probes show marked renal accumulation,[14] raising concerns that strong background signals may occur during tumor imaging.

One strategy to improve the pharmacokinetics of small-molecule radioligands is to introduce a small-molecule albumin binder (ALB).[22] ALB moieties, such as 4-(4-iodophenyl)-butyric acid, have a micromolar affinity for albumin and exhibit reversible binding to albumin in the blood.[23,24] Therefore, the introduction of an ALB moiety may enhance the tumor accumulation and retention and reduce the nontarget binding of ALB-conjugated radioligands that use albumin as a reversible carrier for drug delivery. In the present study, to improve the pharmacokinetics of [^{111}In]In-DO3A-IS1, we designed and synthesized four IS derivatives, which contained 4-(4-substituted phenyl)-moieties as ALB moieties (IS-[^{111}In]In-DO2A-ALB1−4) (Figure 1), and evaluated their utility for imaging tumors that strongly express CA-IX.

EXPERIMENTAL SECTION

General. All reagents were obtained commercially and used without further purification unless otherwise indicated. [^{111}In]-$InCl_3$ was obtained from Nihon Medi-Physics (Tokyo, Japan). ^{1}H and ^{13}C nuclear magnetic resonance (NMR) spectra were recorded on a JNM-ECS400 (JEOL, Tokyo, Japan) with tetramethylsilane as an internal standard. Coupling constants are reported in hertz. Multiplicity was defined as singlet (s), doublet (d), triplet (t), or multiplet (m). Electrospray ionization (ESI) liquid chromatography−mass spectrometry (LC−MS) was conducted with a Shimadzu LCMS-2020 (Shimadzu, Kyoto, Japan). High-resolution mass spectrometry (HRMS) was conducted with an LC−MS-ion trap-time of flight system (Shimadzu). Reversed-phase (RP) high-performance liquid chromatography (HPLC) was performed with a Shimadzu system (an LC-20AT pump with an SPD-20A UV detector, λ = 254 nm; Shimadzu).

Chemistry. *Methyl N^6-(4-(4-Iodophenyl)butanoyl)-L-lysinate (**1**).* First, 4-(4-iodophenyl)butyric acid (116 mg, 0.40 mmol), 1-ethyl-3-(dimethylaminopropyl)carbodiimide (EDC) hydrochloride (153 mg, 0.80 mmol), 1-hydroxybenzotriazole (HOAt) (109 mg, 0.80 mmol), and triethylamine (150 μL, 1.1 mmol) were added to a solution of Boc-Lys(OMe)-OH (118 mg, 0.40 mmol) in *N*,*N*-dimethylformamide (DMF) (20 mL). The mixture was stirred at room temperature overnight. After being lyophilized, trifluoroacetic acid (TFA) (2 mL) was added to the residue. The mixture was stirred at room temperature for 3 h. After the solution was concentrated, the residue was purified by silica gel chromatography ($CHCl_3$/MeOH = 5:1) to give 172 mg of compound **1** (100%). ^{1}H NMR (400 MHz, $CDCl_3$) δ: 7.57 (d, J = 8.4 Hz, 2H), 6.91 (d, J = 8.0 Hz, 2H), 4.03 (s, 1H), 3.77 (s, 3H), 3.20 (s, 2H), 2.54 (t, J = 7.6 Hz, 2H), 2.18 (t, J = 7.4 Hz, 2H), 1.98 (s, 2H), 1.87 (t, J = 7.2 Hz, 2H), 1.50−1.40 (m, 4H). ^{13}C NMR (100 MHz, $CDCl_3$) δ: 173.9, 170.0, 141.1, 137.2 (2C), 130.5 (2C), 90.9, 53.1, 52.8, 38.7, 35.4, 34.5, 29.6, 28.4, 27.0, 21.7. MS (ESI) m/z calculated for $C_{17}H_{26}IN_2O_3^+$ [M + H]$^+$: 433.1; found: 433.1.

*Methyl N^6-(4-(4-Tolyl)butanoyl)-L-lysinate (**2**).* The same reaction used to prepare compound **1** was employed, and 128 mg of compound **2** (100%) was obtained from 4-(4-tolyl)butyric acid. ^{1}H NMR (400 MHz, $CDCl_3$) δ: 8.58 (s, 2H), 7.06 (d, J = 8.4 Hz, 2H), 7.02 (d, J = 8.4 Hz, 2H), 6.43 (s, 1H), 4.02 (t, J = 6.0 Hz, 1H), 3.73 (s, 3H), 3.17 (d, J = 5.2 Hz, 2H), 2.54 (t, J = 7.6 Hz, 2H), 2.29 (s, 3H), 2.17 (t, J = 7.4 Hz, 2H), 1.97 (d, J = 6.4 Hz, 2H), 1.90−1.82 (m, 2H), 1.48 (s, broad, 4H). ^{13}C NMR (100 MHz, $CDCl_3$) δ: 174.0, 169.9, 138.3, 135.2, 128.9 (2C), 128.1 (2C), 53.0, 52.8, 38.6, 35.6, 34.6, 29.6, 28.4, 27.3, 21.8, 20.8. MS (ESI) m/z calculated for $C_{18}H_{29}N_2O_3^+$ [M + H]$^+$: 321.2; found: 321.2.

*Methyl N^6-(4-(4-Bromophenyl)butanoyl)-L-lysinate (**3**).* The same reaction used to prepare compound **1** was employed, and 154 mg of compound **3** (100%) was obtained from 4-(4-bromophenyl)butyric acid. ^{1}H NMR (400 MHz, $CDCl_3$) δ: 8.58 (s, 1H), 7.36 (d, J = 8.0 Hz, 2H), 7.02 (d, J = 8.0 Hz, 2H), 6.58 (t, J = 5.6 Hz, 1H), 4.02 (t, J = 6.4 Hz, 1H), 3.74 (s, 3H), 3.17 (d, J = 5.6 Hz, 2H), 2.54 (t, J = 7.6 Hz, 2H), 2.16 (t, J = 7.6 Hz, 2H), 2.00 (s, 2H), 1.89−1.84 (m, 2H), 1.48 (s, broad, 4H). ^{13}C NMR (100 MHz, $CDCl_3$) δ: 173.9, 170.0, 140.5, 131.2 (2C), 130.1 (2C), 119.5, 53.0, 52.9, 38.7, 35.4, 34.4, 29.6, 28.4, 27.0, 21.7. MS (ESI) m/z calculated for $C_{17}H_{26}BrN_2O_3^+$ [M + H]$^+$: 385.1; found: 385.1.

*Methyl N^6-(4-Phenylbutanoyl)-L-lysinate (**4**).* The same reaction used to prepare compound **1** was employed, and 109 mg of compound **4** (89%) was obtained from 4-phenylbutyric acid. ^{1}H NMR (400 MHz, $CDCl_3$) δ: 8.53 (s, 2H), 7.25−7.11 (m, 5H), 6.74 (t, J = 5.6 Hz, 1H), 4.00 (t, J = 6.4 Hz,1H), 3.69 (s, 3H), 3.14 (d, J = 5.6 Hz, 2H), 2.57 (t, J = 7.6 Hz, 2H), 2.15 (t, J = 7.6 Hz, 2H), 1.94 (s, 2H), 1.90−1.82 (m, 2H), 1.45 (s, broad, 4H). ^{13}C NMR (100 MHz, $CDCl_3$) δ: 173.9, 170.0, 141.5, 128.3 (2C), 128.2 (2C), 125.8, 53.0, 52.8, 38.6, 35.6, 35.1, 29.6, 28.4, 27.2, 21.8. MS (ESI) m/z calculated for $C_{17}H_{27}N_2O_3^+$ [M + H]$^+$: 307.2; found: 307.2.

*(S)-2,2′-(4-(2-((1-Carboxy-5-(4-(4-iodophenyl)-butanamido)pentyl)amino)-2-oxoethyl)-10-(2-oxo-2-((4-(2-sulfamoylimidazo[2,1-b][1,3,4]thiadiazol-6-yl)phenyl)-amino)ethyl)-1,4,7,10-tetraazacyclododecane-1,7-diyl)-diacetic Acid (IS-DO2A-ALB1) (**5**).* First, 2,2′-(4,10-bis(2-(*tert*-butoxy)-2-oxoethyl)-1,4,7,10-tetraazacyclododecane-1,7-diyl)-diacetic acid and 6-(4-aminophenyl)imidazo[2,1-*b*][1,3,4]-thiadiazole-2-sulfonamide were synthesized according to our previous report.[16] Then, 2,2′-(4,10-bis(2-(*tert*-butoxy)-2-oxoethyl)-1,4,7,10-tetraazacyclododecane-1,7-diyl)diacetic acid (103 mg, 0.20 mmol), EDC hydrochloride (38 mg, 0.20 mmol), HOAt (27 mg, 0.20 mmol), and triethylamine (27 μL,

https://dx.doi.org/10.1021/acs.molpharmaceut.0c00953
Mol. Pharmaceutics XXXX, XXX, XXX−XXX

0.20 mmol) were added to a solution of compound **1** (86 mg, 0.20 mmol) in DMF (5 mL). The mixture was stirred at room temperature for 24 h. Then, 6-(4-aminophenyl)imidazo[2,1-*b*][1,3,4]thiadiazole-2-sulfonamide (59 mg, 0.20 mmol), EDC hydrochloride (38 mg, 0.20 mmol), HOAt (27 mg, 0.20 mmol), and triethylamine (27 μL, 0.20 mmol) were added. After being stirred at room temperature for 24 h, the solution was lyophilized. HCl (6 N, 2 mL) was slowly added to the resultant residue in an ice bath. After being stirred at room temperature for 12 h, the solution was concentrated. The residue was purified by RP-HPLC with a Cosmosil C_{18} column ($5C_{18}$-AR-II, 20 × 250 mm; Nacalai Tesque, Kyoto, Japan) at a flow rate of 5.0 mL/min using H_2O/MeCN/TFA [85:15:0.1 (0 min) to 55:45:0.1 (120 min)] as a solvent (the mobile phase) to give 2.5 mg of compound **5** (1.2%). HRMS (ESI) *m/z* calculated for $C_{42}H_{56}IN_{11}NaO_{11}S_2^+$ $[M + Na]^+$: 1104.2539; found: 1104.2458.

*(S)-2,2′-(4-(2-((1-Carboxy-5-(4-(4-tolyl)butanamido)-pentyl)amino)-2-oxoethyl)-10-(2-oxo-2-((4-(2-sulfamoylimidazo[2,1-b][1,3,4]thiadiazol-6-yl)phenyl)-amino)ethyl)-1,4,7,10-tetraazacyclododecane-1,7-diyl)-diacetic Acid (IS-DO2A-ALB2) (**6**).* The same reaction used to prepare compound **5** was employed, and 1.3 mg of compound **6** (0.6%) was obtained from compound **2**. HRMS (ESI) *m/z* calculated for $C_{43}H_{60}N_{11}O_{11}S_2^+$ $[M + H]^+$: 970.3910; found: 970.3911.

*(S)-2,2′-(4-(2-((5-(4-(4-Bromophenyl)butanamido)-1-carboxypentyl)amino)-2-oxoethyl)-10-(2-oxo-2-((4-(2-sulfamoylimidazo[2,1-b][1,3,4]thiadiazol-6-yl)phenyl)-amino)ethyl)-1,4,7,10-tetraazacyclododecane-1,7-diyl)-diacetic Acid (IS-DO2A-ALB3) (**7**).* The same reaction used to prepare compound **5** was employed, and 3.0 mg of compound **7** (1.5%) was obtained from compound **3**. HRMS (ESI) *m/z* calculated for $C_{42}H_{56}BrN_{11}NaO_{11}S_2^+$ $[M + Na]^+$: 1056.2678; found: 1056.2665.

*(S)-2,2′-(4-(2-((1-Carboxy-5-(4-phenylbutanamido)-pentyl)amino)-2-oxoethyl)-10-(2-oxo-2-((4-(2-sulfamoylimidazo[2,1-b][1,3,4]thiadiazol-6-yl)phenyl)-amino)ethyl)-1,4,7,10-tetraazacyclododecane-1,7-diyl)-diacetic Acid (IS-DO2A-ALB4) (**8**).* The same reaction used to prepare compound **5** was employed, and 3.0 mg of compound **8** (1.7%) was obtained from compound **4**. HRMS (ESI) *m/z* calculated for $C_{42}H_{58}N_{11}O_{11}S_2^+$ $[M + H]^+$: 956.3753; found: 956.3760.

*IS-[^{mat}In]In-DO2A-ALB1 (**9**).* $InCl_3$ anhydrous (10 eq) was added to a solution of compound **5** in 2-(*N*-morpholino)-ethanesulfonic acid (MES) buffer (0.1 M, pH 5.5, 300 μL). The mixture was stirred at 60 °C overnight. After being concentrated, the mixture was purified by RP-HPLC with a Cosmosil C_{18} column ($5C_{18}$-AR-II, 20 × 250 mm; Nacalai Tesque) at a flow rate of 5.0 mL/min using H_2O/MeCN/TFA [85:15:0.1 (0 min) to 55:45:0.1 (60 min)] as a solvent (the mobile phase) to give compound **9**. HRMS (ESI) *m/z* calculated for $C_{42}H_{54}I^{115}InN_{11}O_{11}S_2^+$ $[M]^+$: 1194.1524; found: 1194.1541.

*IS-[^{mat}In]In-DO2A-ALB2 (**10**).* The same reaction used to prepare compound **9** was employed, and compound **10** was obtained from compound **6**. HRMS (ESI) *m/z* calculated for $C_{43}H_{57}{}^{115}InN_{11}O_{11}S_2^+$ $[M]^+$: 1082.2714; found: 1082.2590.

*IS-[^{mat}In]In-DO2A-ALB3 (**11**).* The same reaction used to prepare compound **9** was employed, and compound **11** was obtained from compound **7**. HRMS (ESI) *m/z* calculated for $C_{42}H_{54}Br^{115}InN_{11}O_{11}S_2^+$ $[M]^+$: 1146.1662; found: 1146.1675.

*IS-[^{mat}In]In-DO2A-ALB4 (**12**).* The same reaction used to prepare compound **9** was employed, and compound **12** was obtained from compound **8**. HRMS (ESI) *m/z* calculated for $C_{42}H_{55}{}^{115}InN_{11}O_{11}S_2^+$ $[M]^+$: 1068.2557; found: 1068.2548.

Radiolabeling. An $[^{111}In]InCl_3$ (100 μL, 3.7 MBq) solution was mixed with an acetate buffer (0.1 M, pH 4.6, 200 μL) and preincubated at room temperature for 10 min. Ten microliters of the precursor (compound **5**, **6**, **7**, or **8**) in dimethyl sulfoxide (1 mM) was added to this solution, and the mixture was incubated at 90 °C for 30 min. After being cooled to room temperature, the mixture was purified by RP-HPLC on a Cosmosil C_{18} column ($5C_{18}$-AR-II, 4.6 × 150 mm; Nacalai Tesque) with H_2O/MeCN/TFA used as a solvent (the mobile phase) [85:15:0.1 (0 min) to 70:30:0.1 (60 min)] at a flow rate of 1.0 mL/min.

Measurement of Partition Coefficients. The experimental determination of partition coefficients was performed in 1-octanol and phosphate-buffered saline (PBS) (pH 7.4). 1-Octanol (3 mL) and PBS (3 mL) were pipetted into a 15 mL test tube containing IS-[^{111}In]In-DO2A-ALB1−4 (740 kBq). The test tube was vortexed for 2 min and then centrifuged (4000*g*, 5 min). Aliquots (0.5 mL) from the 1-octanol and PBS phases were transferred into two test tubes for counting. The amount of radioactivity in each tube was measured with a γ counter (Wallac 2470 Wizard; PerkinElmer, Waltham, MA, USA). The partition coefficient was calculated using the following equation: $\log P_{ow} = \log[\text{count}_{1\text{-octanol}}/\text{count}_{PBS}]$.

Animals. All animal experiments were performed in accordance with our institutional guidelines and were approved by the Kyoto University Animal Care Committee (ethics approval number: 20-20). Male BALB/c-*nu*/*nu* nude mice and male ddY mice were purchased from Japan SLC (Shizuoka, Japan). The animals were housed in a sterile environment under a 12 h light−dark cycle, were fed standard chow, and had free access to water. All efforts were made to minimize suffering.

Cell Culture. HT-29 and MDA-MB-231, which are human colorectal cancer cell and human breast cancer cell lines, respectively, were purchased from Sumitomo Dainippon Pharma (Osaka, Japan). The cells were maintained in Dulbecco's modified Eagle's medium (DMEM) (Nacalai Tesque) supplemented with 10% heat-inactivated fetal bovine serum (Thermo Fisher Scientific, Waltham, MA, USA), 100 U/mL penicillin, and 100 μg/mL streptomycin at 37 °C in an atmosphere containing 5% CO_2.

***In Vitro* Cell-Binding Assay.** HT-29 and MDA-MB-231 cells were incubated in 12-well plates (4×10^5 cells/well) at 37 °C in an atmosphere containing 5% CO_2 for 24 h. After removing the medium, IS-[^{111}In]In-DO2A-ALB1−4 or [^{111}In]In-DO3A-IS1 (37 kBq) in DMEM (1 mL) with or without human serum albumin (HSA) (1 mg) was added to each well, and the plates were incubated at 37 °C in an atmosphere containing 5% CO_2 for 2 h. The half-maximal inhibitory concentration (IC_{50}) was calculated by adding increasing concentrations (5.1 pM−50 μM) of acetazolamide to the HT-29 cell culture. After incubation, the wells were rinsed with 1 mL of PBS (pH 7.4) (Nacalai Tesque), and the cells were lysed with 1 N NaOH (0.2 mL × 2). The radioactivity in the cell solution was measured with a γ counter (PerkinElmer). The protein concentration of the cell solution was determined using a bicinchoninic acid protein assay kit (Thermo Fisher Scientific).

https://dx.doi.org/10.1021/acs.molpharmaceut.0c00953
Mol. Pharmaceutics XXXX, XXX, XXX−XXX

Scheme 1. Synthetic Routes for ALB-Conjugated IS Derivatives

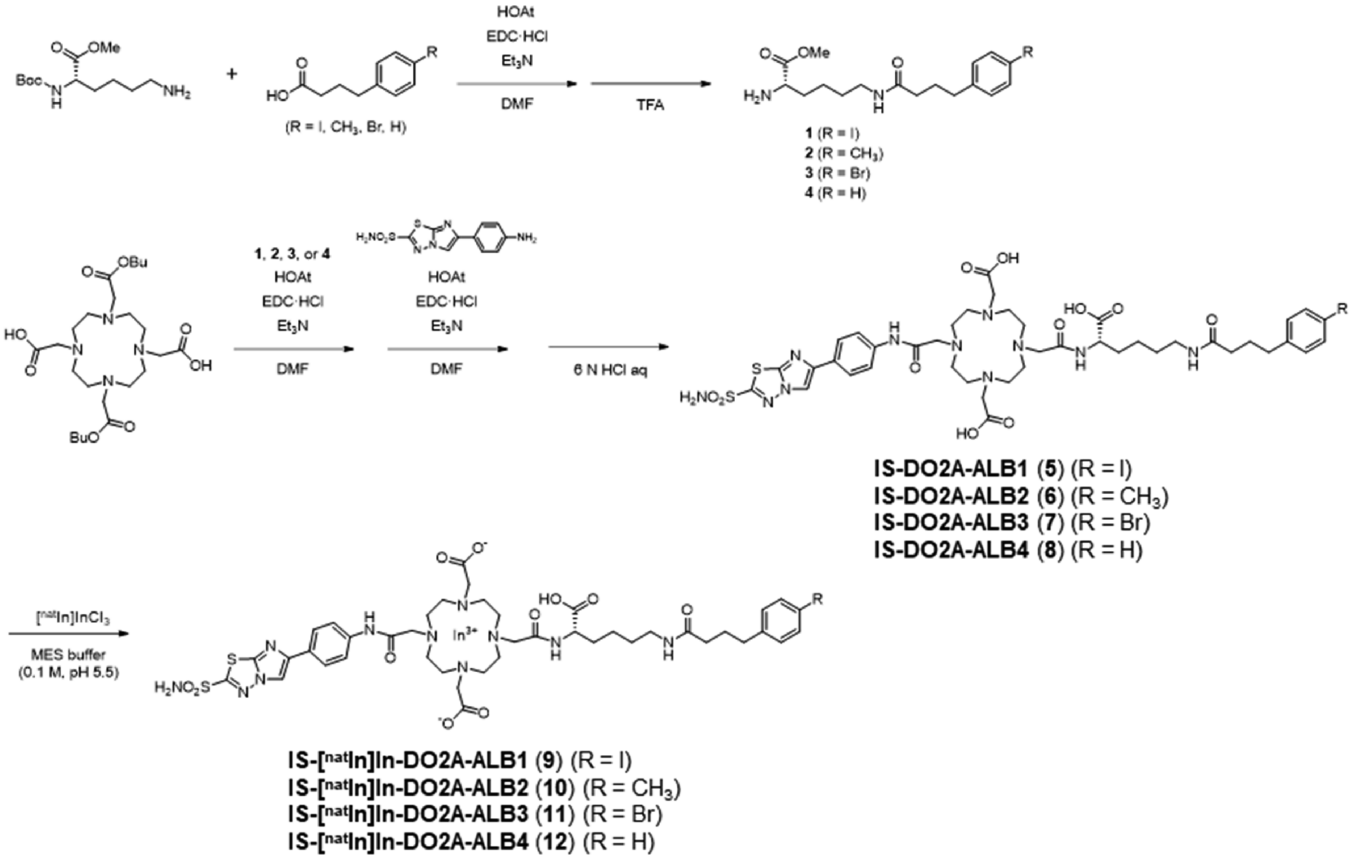

Protein-Binding Assay. Human plasma was purchased from Cosmo Bio (Tokyo, Japan). Mouse plasma was obtained by centrifuging mouse blood (ddY mouse, male, 5 weeks old) in venous blood collection tubes (Becton, Dickinson and Company, Franklin Lakes, NJ, USA). A solution of IS-[^{111}In]In-DO2A-ALB1−4 or [^{111}In]In-DO3A-IS1 (37 kBq) in PBS (50 μL) was added to 200 μL of PBS, human plasma, mouse plasma, or HSA solution (45 mg in 1 mL of PBS, which was based on the approximate physiological concentration of HSA). After being vortexed, the solution was incubated at 37 °C for 10 min. Then, after incubation, 100 μL of the solution was loaded onto a gel filtration column (Sephadex G-50 Fine; Cytiva, Tokyo, Japan) with 0.1 M acetate buffer (pH 6.0) followed by centrifugation (1500*g*, 2 min). The radioactivity of the column and eluate was then measured with a γ counter (PerkinElmer).

Tumor Model. Under isoflurane-induced anesthesia (2% isoflurane in an air mixture), BALB/c-*nu*/*nu* nude mice (male, 5 weeks old) were subcutaneously inoculated (in the shoulder) with HT-29 cells (5×10^6 cells/mouse) or MDA-MB-231 cells (1×10^7 cells/mouse) in 150 μL of DMEM and Geltrex (Thermo Fisher Scientific) at a 1:1 ratio. All efforts were made to minimize suffering.

Biodistribution Study Involving HT-29 Tumor-Bearing Mice. A saline solution (100 μL) of IS-[^{111}In]In-DO2A-ALB1−4 (259 kBq) containing L-ascorbic acid (3 mg) or a saline solution (100 μL) of [^{111}In]In-DO3A-IS1 (259 kBq) containing L-ascorbic acid (1 mg) was directly injected into the tail vein of HT-29 tumor-bearing mice (n = 5 in each group). The mice were sacrificed at 1, 4, 8, 24, 48, 96, or 192 h postinjection, and then the organs and tissues of interest were collected. Each organ was weighed and radioactivity was measured using a γ counter (PerkinElmer). The % injected activity/g of the samples was calculated by comparing the sample counts with the injected activity count. Area under the curve (AUC) values were determined for the radioactivity in the blood, kidneys, and tumors after the injection of IS-[^{111}In]In-DO2A-ALB1−4 or [^{111}In]In-DO3A-IS1 based on non-decay-corrected biodistribution data using the GraphPad Prism software.

Biodistribution Study Involving MDA-MB-231 Tumor-Bearing Mice. A saline solution (100 μL) of IS-[^{111}In]In-DO2A-ALB1 (259 kBq) containing L-ascorbic acid (3 mg) was directly injected into the tail vein of MDA-MB-231 tumor-bearing mice (n = 5). The mice were sacrificed at 48 h postinjection, and then the organs and tissues of interest were collected. Each organ was weighed and radioactivity was measured using a γ counter (PerkinElmer). The % injected activity/g of the samples was calculated by comparing the sample counts with the injected activity count.

SPECT/CT of HT-29 or MDA-MB-231 Tumor-Bearing Mice. A saline solution (150 μL) of IS-[^{111}In]In-DO2A-ALB1 (7.6−8.0 MBq) containing L-ascorbic acid (3 mg) was injected into the tail vein of BALB/c *nu*/*nu* mice with HT-29 or MDA-MB-231 tumors. The mice were anesthetized using isoflurane (2% in an air mixture). SPECT and CT images of the mice were obtained at 4, 24, and 48 h postinjection using a Triumph combined PET/SPECT/CT system (TriFoil Imaging, Chatsworth, CA, USA) with 1.0 mm pinhole collimators, and the images were reconstructed using the ordered subset expectation maximization (OSEM) method according to a previous report.[25] In addition, a saline solution (150 μL) of [^{111}In]In-

https://dx.doi.org/10.1021/acs.molpharmaceut.0c00953
Mol. Pharmaceutics XXXX, XXX, XXX−XXX

Scheme 2. ^{111}In-Labeling of ALB-Conjugated IS Derivatives

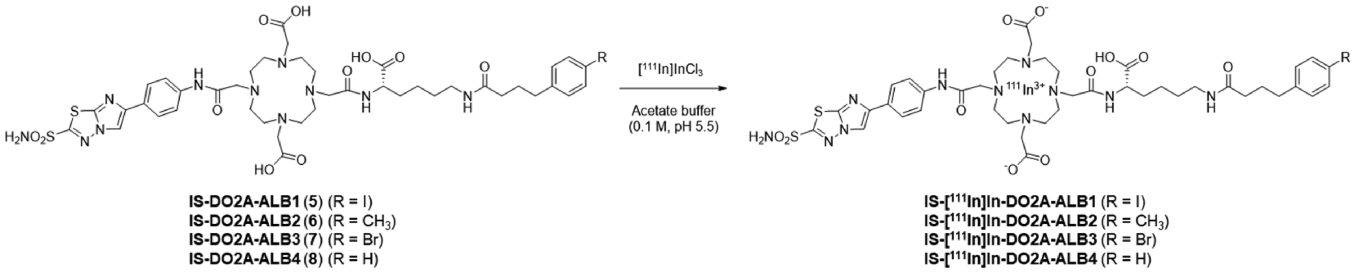

IS-DO2A-ALB1 (5) (R = I)
IS-DO2A-ALB2 (6) (R = CH_3)
IS-DO2A-ALB3 (7) (R = Br)
IS-DO2A-ALB4 (8) (R = H)

IS-[^{111}In]In-DO2A-ALB1 (R = I)
IS-[^{111}In]In-DO2A-ALB2 (R = CH_3)
IS-[^{111}In]In-DO2A-ALB3 (R = Br)
IS-[^{111}In]In-DO2A-ALB4 (R = H)

DO3A-IS1 (23−29 MBq) was injected into the tail vein of BALB/c *nu/nu* mice with HT-29 tumors. SPECT and CT images were obtained at 24 h postinjection using the U-SPECT-II system (MILabs, Utrecht, the Netherlands) with 1.0 mm pinhole collimators, and the images were reconstructed using the OSEM method. The acquired SPECT and CT data were analyzed using the PMOD software (version 3.3; PMOD Technologies, Zürich, Switzerland).

Statistical Analysis. All data were analyzed with GraphPad Prism or Microsoft Excel. Differences at the 95% confidence level ($P < 0.05$) according to the two-tailed Student *t* test were considered significant.

RESULTS

Chemistry and Radiolabeling. The synthetic pathways for IS-DO2A-ALB1−4 (compounds **5**−**8**) and the corresponding nonradioactive indium complexes (compounds **9**−**12**) are outlined in Scheme 1. After the introduction of the relevant ALB moiety (compounds **1**−**4**) into 2,2′-(4,10-bis(2-(*tert*-butoxy)-2-oxoethyl)-1,4,7,10-tetraazacyclododecane-1,7-diyl)-diacetic acid, 6-(4-aminophenyl)imidazo[2,1-*b*][1,3,4]-thiadiazole-2-sulfonamide[16] was conjugated with the carboxylic acid on the opposite side using EDC and HOAt. After that, the precursors (compounds **5**−**8**) were prepared by subjecting *tert*-butyl and methyl ester to deprotection. Compounds **9**−**12** were synthesized from compounds **5**−**8** through chelation reactions with $InCl_3$ and 0.1 M MES buffer (pH 5.5).

^{111}In-labeling was carried out by incubating the precursors with [^{111}In]$InCl_3$ in 0.1 M acetate buffer (pH 5.5) at 90 °C (Scheme 2). After RP-HPLC-based purification, IS-[^{111}In]In-DO2A-ALB1−4 were obtained with high radiochemical purity (>95%), as determined by RP-HPLC. They were synthesized at radiochemical yields of 31−44%. The radiochemical identities of IS-[^{111}In]In-DO2A-ALB1−4 were verified by comparative RP-HPLC, with the corresponding ^{nat}In complex used as a reference (Figure S1). The molar activity of these tracers was calculated to range from 22 to 87 GBq/μmol.

***In Vitro* Cell-Binding Assay.** A cell-binding assay was performed to evaluate the ability of IS-[^{111}In]In-DO2A-ALB1−4 and [^{111}In]In-DO3A-IS1 to bind to CA-IX-expressing cells *in vitro* (Figure S2). Based on the findings of our previous study, HT-29 and MDA-MB-231 cells were used as cells with high and low CA-IX expression levels, respectively.[19] A fixed concentration of the ^{111}In complex and increasing concentrations of nonradioactive acetazolamide, a classical CA inhibitor, were incubated with HT-29 cells, and then the IC_{50} value for acetazolamide was determined in the presence of each ^{111}In complex. A higher IC_{50} value for acetazolamide indicated that the radiotracer bound to the cells to a greater extent. IS-[^{111}In]In-DO2A-ALB1−4 and [^{111}In]In-DO3A-IS1 bound to HT-29 cells to a similar extent in the absence of acetazolamide (300−400% initial activity/mg protein). Acetazolamide showed an IC_{50} value of 127 ± 20 nM in the presence of [^{111}In]In-DO3A-IS1, while values of 105−574 nM were observed in the presence of IS-[^{111}In]In-DO2A-ALB1−4 (Table 1), indicating that the ALB-conjugated IS derivatives bound to the cells to a comparable or greater degree than [^{111}In]In-DO3A-IS1. Conventional saturation binding assays using nonradioactive test compounds were not performed owing to the low yields of the ^{nat}In complexes. However, the competition binding assay conducted with nonradioactive acetazolamide in this study allowed the determination of IC_{50} values and suggested that IS-[^{111}In]In-DO2A-ALB1−4 exhibited a high affinity for HT-29 cells. Moreover, the IC_{50} value for acetazolamide seen in the presence of IS-[^{111}In]In-DO2A-ALB1, which bound to HT-29 cells to a greater extent than the other radiotracers, was also evaluated in a medium containing HSA to assess the effects of the presence of HSA on binding to CA-IX. The IC_{50} value obtained in the presence of HSA was 101 ± 63 nM, which was lower than that without HSA (574 ± 53 nM) and comparable to that of the compound without an ALB moiety ([^{111}In]DO3A-IS1, 127 ± 20 nM) (Table S1), indicating that the binding of IS-[^{111}In]In-DO2A-ALB1 to its target cells was slightly decreased in the presence of HSA. In addition, IS-[^{111}In]In-DO2A-ALB1 exhibited a more selective binding to HT-29 cells (396% initial activity/mg protein) than the MDA-MB-231 cells (52.8% initial activity/mg protein), which expressed CA-IX at low levels (Figure S3).

Table 1. Half-Maximal Inhibitory Concentration (IC_{50}, nM) for the Binding of Acetazolamide to HT-29 Cells Determined Using IS-[^{111}In]In-DO2A-ALB1−4 and [^{111}In]In-DO3A-IS1 as Ligands[a]

compound	IC_{50} for acetazolamide (nM)
IS-[^{111}In]In-DO2A-ALB1	574 ± 53
IS-[^{111}In]In-DO2A-ALB2	165 ± 61
IS-[^{111}In]In-DO2A-ALB3	288 ± 46
IS-[^{111}In]In-DO2A-ALB4	105 ± 8.0
[^{111}In]In-DO3A-IS1	127 ± 20

[a]Values are expressed as the mean ± standard deviation for six independent experiments.

Protein-Binding Assay. The binding of the ALB-conjugated IS derivatives to plasma proteins was evaluated by gel filtration chromatography (Figure S4). After being incubated in PBS, none of the IS derivatives produced marked radioactivity in the eluent fraction containing high-molecular-weight compounds. On the other hand, incubating them in human or mouse plasma resulted in increased radioactivity in the eluent for all IS derivatives, suggesting that the IS derivatives had bound to plasma proteins. Among the four

https://dx.doi.org/10.1021/acs.molpharmaceut.0c00953
Mol. Pharmaceutics XXXX, XXX, XXX−XXX

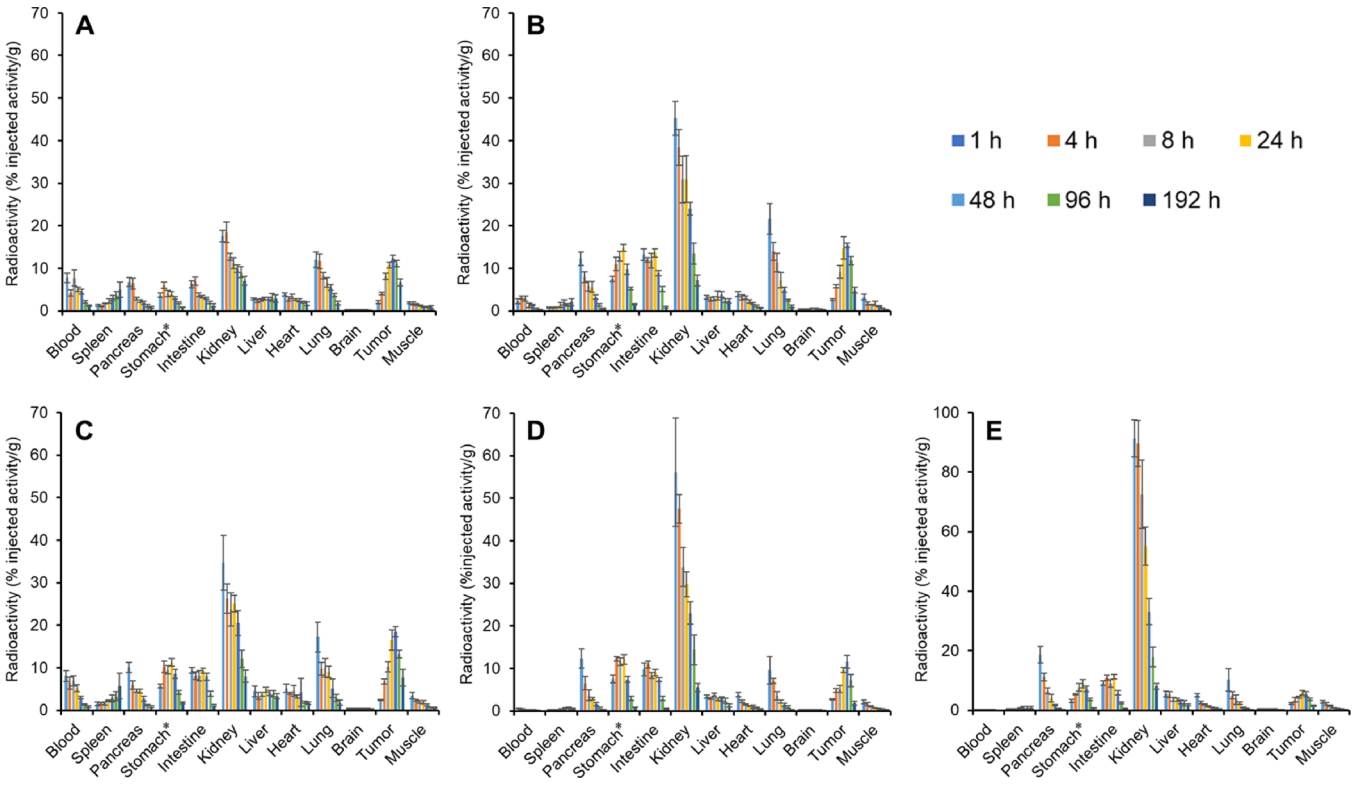

Figure 2. *In vivo* biodistribution study of IS-[^{111}In]In-DO2A-ALB1 (A), IS-[^{111}In]In-DO2A-ALB2 (B), IS-[^{111}In]In-DO2A-ALB3 (C), IS-[^{111}In]In-DO2A-ALB4 (D), and [^{111}In]In-DO3A-IS1 (E) using HT-29 tumor-bearing mice. Values are expressed as % injected activity per gram of organ tissue. Each value represents the mean ± standard deviation for five mice. *Values are expressed as % injected activity.

compounds, IS-[^{111}In]In-DO2A-ALB1 showed the highest degree of binding to human and mouse plasma proteins (both 93%), while IS-[^{111}In]In-DO2A-ALB4 showed the lowest level of binding to such proteins (48 and 43%, respectively), indicating that the substituted group within the ALB moiety (I, CH_3, Br, or H) has a critical effect on protein binding. However, the IS derivative without an ALB moiety ([^{111}In]In-DO3A-IS1) also bound to human and mouse proteins (53 and 61%, respectively), suggesting that the IS scaffold binds to such proteins. After incubation in HSA solution, IS-[^{111}In]In-DO2A-ALB1−3 showed marked protein binding (90−95%); however, IS-[^{111}In]In-DO2A-ALB4 showed a slightly lower protein binding (74%), and [^{111}In]In-DO3A-IS1 demonstrated a relatively low level of protein binding (22%), suggesting that the introduction of an ALB moiety had an effect on the binding of the derivatives to proteins.

Biodistribution. A biodistribution study was carried out using HT-29 tumor-bearing mice to evaluate the *in vivo* biodistributions of the ^{111}In-labeled IS derivatives (Figure 2, Figure S5, and Tables S2−S6). High and low levels of CA-IX expression were detected in HT-29 and MDA-MB-231 tumors, respectively, in our previous study.[19] Compared with that exhibited by [^{111}In]In-DO3A-IS1 (0.14% injected activity/g at 1 h postinjection), the blood retention of the derivatives was markedly increased by the introduction of ALB-I, -CH_3, or -Br (2.22−8.03% injected activity/g at 1 h postinjection). However, the introduction of ALB-H did not cause a marked retention of radioactivity in the blood (0.56% injected activity/g at 1 h postinjection). These findings corresponded with the ability of each moiety to bind to HSA *in vitro* (Figure S4). In addition, compared with the tumor uptake of [^{111}In]In-DO3A-IS1 (1.49−5.92% injected activity/g at 1−192 h postinjection), the introduction of the ALB moieties significantly increased the tumor uptake of the derivatives (11.54−18.49% injected activity/g at 48 h postinjection), although IS-[^{111}In]In-DO2A-ALB4 showed no marked retention in the blood. IS-[^{111}In]In-DO2A-ALB3 exhibited the greatest tumor accumulation (Figure S5), while IS-[^{111}In]In-DO2A-ALB1 bound to the HT-29 cells to a greater extent than the other radiotracers *in vitro* (Table 1). At 1 h postinjection, IS-[^{111}In]In-DO2A-ALB1−4 exhibited a significantly lower renal accumulation (17.55−56.06% injected activity/g) than [^{111}In]In-DO3A-IS1 (91.30% injected activity/g), suggesting that the ALB moieties had powerful effects on renal accumulation. IS-[^{111}In]In-DO2A-ALB1, which showed the greatest degree of plasma protein binding, demonstrated the highest tumor/kidney ratio at all evaluated time points among the four compounds, and the value of this ratio was around 1 at 24−192 h postinjection (Figure S5). On the other hand, IS-[^{111}In]In-DO2A-ALB1 remained in the blood the longest; however, its tumor/blood ratio was ≥1 at 4 h postinjection, which would allow it to be used for *in vivo* tumor-specific imaging. These results indicate that IS-[^{111}In]In-DO2A-ALB1 is the most useful of the examined agents for *in vivo* diagnostic imaging of tumors. Moreover, we performed a biodistribution study using male mice with MDA-MB-231 tumors to evaluate the selectivity of the radiotracers for CA-IX-expressing tumors. We used male mice as we also used male mice to evaluate [^{111}In]In-DO3A-IS1 in our previous study,[16] and the incidence of breast cancer in males is approximately 1%. The HT-29 tumors exhibited a greater IS-[^{111}In]In-DO2A-ALB1 uptake (12.32% injected activity/g at 48 h postinjection) than the MDA-MB-231 tumors (5.05% injected activity/g) (Figure S6 and Table S7).

https://dx.doi.org/10.1021/acs.molpharmaceut.0c00953
Mol. Pharmaceutics XXXX, XXX, XXX−XXX

In comparison with the AUC values of [^{111}In]In-DO3A-IS1, IS-[^{111}In]In-DO2A-ALB1−3 exhibited markedly increased tumor AUC values (375.6 vs 869.9−1189) and blood AUC values (60.33 vs 158.2−393.1) and markedly decreased kidney AUC values (3266 vs 893.7−1919) until 192 h postinjection (Figure S7 and Table S8), indicating the marked effects of these ALB moieties. The increased blood AUC values are a problem in terms of the radiation burden; however, the markedly decreased kidney AUC values may minimize radiotoxicity to the kidneys, where the ^{111}In-labeled IS derivatives mainly accumulated. Only IS-[^{111}In]In-DO2A-ALB1 showed a tumor/kidney AUC ratio (0.973) of almost 1, suggesting that the ALB-I moiety has the greatest clinical potential.

SPECT/CT. A SPECT study of HT-29 or MDA-MB-231 tumor-bearing mice was performed with IS-[^{111}In]In-DO2A-ALB1 (Figure 3 and Figure S8). In our previous study, SPECT

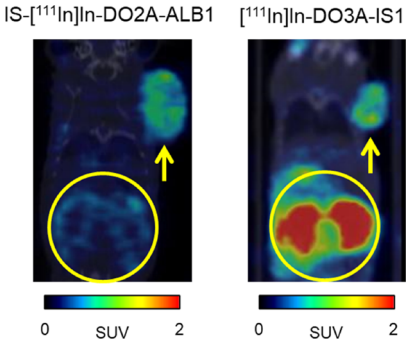

Figure 3. Coronal SPECT/CT images of an HT-29 tumor-bearing mouse obtained at 24 h postinjection using IS-[^{111}In]In-DO2A-ALB1 or [^{111}In]In-DO3A-IS1. Yellow arrows and circles indicate HT-29 tumors and kidneys, respectively.

with [^{111}In]In-DO3A-IS1 provided clear imaging of HT-29 tumors; however, a marked accumulation of [^{111}In]In-DO3A-IS1 was observed in the kidneys.[16] In contrast, IS-[^{111}In]In-DO2A-ALB1 resulted in HT-29 tumors being clearly visualized, while no marked radioactivity was observed in the kidneys (Figure 3). These findings corresponded with those of the biodistribution study (Figure 2). Moreover, IS-[^{111}In]In-DO2A-ALB1 exhibited more marked accumulation in the HT-29 tumors than in the MDA-MB-231 tumors (Figure S8). A maximum intensity projection of the whole body is shown in Figure S9.

DISCUSSION

The kidneys are critical organs for small-molecule radioligands since marked renal accumulation may cause strong background signals and a high radiation burden.[26] However, small-molecule radioligands, especially those targeting CA-IX, the folate receptor (FR), or prostate-specific membrane antigen (PSMA), often show marked accumulation in the kidneys due to their clearance through the urinary tract and the expression of endogenous receptors (isoforms) within the kidneys.[14,27,28] Recently, the introduction of ALB moieties into radioligands has attracted much attention as a strategy for decreasing nonspecific uptake in normal organs and increasing specific uptake in tumors.[22] Müller et al. reported an ALB-conjugated folate-based radioligand that showed a lower renal accumulation than a corresponding folate-based radioligand without an ALB moiety.[29] The effects of the conjugation of ALB moieties to the FR and PSMA ligands have been well evaluated;[22,29−34] however, no study has examined the effects of ALB moieties on CA-IX ligands.

Among several previously reported ALB moieties,[23] 4-(4-iodophenyl)butyric acid and truncated Evans blue entities have been attached to many radioligands as ALB moieties.[22] Selecting appropriate ALB moieties for radioligands is critical since they may cause marked changes in the pharmacokinetics of radioligands, including tumor and renal accumulation.[30,34] The introduction of an ALB moiety does not necessarily cause a reduction in renal accumulation, especially for PSMA ligands.[31−33] Thus, ALB moieties should be carefully selected for each radioligand to reduce background (renal) accumulation while increasing tumor accumulation. To explore the optimal ALB moiety for tumor imaging, in this study, we selected four ALB moieties [4-(4-iodophenyl), 4-(4-tolyl), 4-(4-bromophenyl), and 4-phenyl] with different affinities for albumin[23] and conjugated each ALB moiety to [^{111}In]In-DO3A-IS1, which demonstrated favorable tumor accumulation but marked renal accumulation in our previous study.

The hydrophilicity of ^{111}In complexes was evaluated by measuring the partition coefficients using 1-octanol and PBS (Table S9). Hydrophilicity was decreased by the introduction of an ALB moiety, and IS-[^{111}In]In-DO2A-ALB1, in which 4-(4-iodophenyl) was used as the ALB moiety, exhibited the lowest hydrophilicity (−1.70 ± 0.01). In *in vitro* assays, IS-[^{111}In]In-DO2A-ALB1−4 bound to HSA to a greater extent than [^{111}In]In-DO3A-IS1 (Figure S4), but binding to target cells was not decreased (Table 1). Dumelin et al. reported that 4-(4-iodophenyl), 4-(4-tolyl), and 4-(4-bromophenyl) had a moderate affinity for HSA in isothermal titration calorimetry studies conducted in a solution (K_d = 3.2, 52, and 30 μM, respectively).[23] In addition, a chromatographic albumin binding assay indicated that the HSA-binding activity of the four ALB moieties that we selected for this study exhibited the following order: 4-(4-iodophenyl) > 4-(4-bromophenyl) > 4-(4-tolyl) > 4-phenyl.[23] The results of the protein-binding assay in the present study using HSA were consistent with those of previously reported binding experiments (IS-[^{111}In]In-DO2A-ALB1−3, 90−95%; IS-[^{111}In]In-DO2A-ALB4, 74%), while [^{111}In]In-DO3A-IS1 (which did not have an ALB moiety) showed no marked binding to HSA (22%). Moreover, the ability of the derivatives to bind to HSA partially corresponded with their hydrophilicity; i.e., the IS derivatives with lower hydrophilicity bound to HSA to a greater extent. This suggests that hydrophilicity is related to the nonspecific binding to albumin to some extent *in vitro*.

IS-[^{111}In]In-DO2A-ALB1−4 showed marked HT-29 tumor accumulation at 24 h postinjection (9.61−16.48% injected activity/g). Indeed, their tumor accumulation was much greater than that of previously reported CA-IX radioligands, including [^{111}In]In-DO3A-IS1.[16−21] Several PSMA radioligands have demonstrated increased tumor and renal accumulation after the introduction of an ALB moiety.[31−33] In the current study, the ALB-conjugated IS derivatives showed higher tumor accumulation and lower renal accumulation than [^{111}In]In-DO3A-IS1. Blood retention was also increased by the introduction of ALB moieties into the IS derivatives; however, all of the IS derivatives showed blood retention values of <10% injected activity/g, while ALB-conjugated PSMA radioligands exhibited blood retention values of >10% injected activity/g at 1 h postinjection,[31−33] indicating the utility of ALB-conjugated IS derivatives for

https://dx.doi.org/10.1021/acs.molpharmaceut.0c00953
Mol. Pharmaceutics XXXX, XXX, XXX−XXX

diagnostic imaging. The reduction in renal accumulation caused by ALB moieties may be due to the decreased rates of filtration and reabsorption in the proximal renal tubules,[35,36] which may also limit the access of radioligands to other CA isozymes expressed in the kidneys.

This is the first study to demonstrate the utility of introducing ALB moieties into CA-IX radioligands for reducing their renal accumulation and increasing their tumor accumulation. The results indicate that the introduction of ALB moieties into pharmaceuticals targeting CA-IX is a powerful strategy for improving their pharmacokinetics, which may contribute to not only *in vivo* diagnostic imaging but also treatments, such as targeted radionuclide therapies that do not produce critical toxicities affecting normal organs. However, the introduction of ALB moieties led to not only markedly decreased kidney AUC values but also increased blood AUC values, raising concerns about hematological toxicities, especially during targeted radionuclide therapy. A series of ALB moieties with various affinities for albumin have been reported;[22] thus, the selection of the optimal ALB moiety for each case may lead to personalized radiotheranostics with maximal effects on tumors and minimal radiotoxicity, especially in the kidneys and blood.

CONCLUSIONS

Based on the findings of our previous study in which [^{111}In]In-DO3A-IS1 exhibited marked tumor accumulation but also marked renal accumulation, we synthesized IS-[^{111}In]In-DO2A-ALB1−4, which included four different ALB moieties, and evaluated their utility for CA-IX-SPECT imaging. IS-[^{111}In]In-DO2A-ALB1−4 bound to HSA to a greater extent than [^{111}In]In-DO3A-IS1, while their binding to HT-29 cells was not decreased *in vitro*. The introduction of the ALB moieties into the ^{111}In-labeled IS derivatives markedly decreased their renal accumulation while increasing their tumor accumulation and blood retention. In addition, the kind of ALB moiety used markedly influenced the pharmacokinetics of the ^{111}In-labeled IS derivatives. IS-[^{111}In]In-DO2A-ALB1 showed the highest tumor/kidney ratio but remained in the blood the longest. In contrast, IS-[^{111}In]In-DO2A-ALB4 showed the lowest tumor/kidney ratio and did not exhibit marked blood retention. IS-[^{111}In]In-DO2A-ALB3 displayed the greatest uptake by the HT-29 tumors, and marked amounts remained in the blood. SPECT imaging with IS-[^{111}In]In-DO2A-ALB1 clearly depicted tumors that strongly expressed CA-IX without marked background signals. These results indicate that IS-[^{111}In]In-DO2A-ALB1 may be an effective CA-IX imaging probe and that the introduction of ALB moieties may improve the pharmacokinetics of CA-IX ligands.

ASSOCIATED CONTENT

Supporting Information

The Supporting Information is available free of charge at https://pubs.acs.org/doi/10.1021/acs.molpharmaceut.0c00953.

Co-injection HPLC profiles of IS-[$^{nat/111}$In]In-DO2A-ALB1−4 (Figure S1), inhibition curves of binding of IS-[^{111}In]In-DO2A-ALB1−4 and [^{111}In]In-DO3A-IS1 to HT-29 cells (Figure S2), IC_{50} values for acetazolamide in the presence of IS-[^{111}In]In-DO2A-ALB1 and [^{111}In]In-DO3A-IS1 with or without HSA (Table S1), binding of IS-[^{111}In]In-DO2A-ALB1 to HT-29 and MDA-MB-231 cells (Figure S3), plasma protein binding of IS-[^{111}In]In-DO2A-ALB1−4 and [^{111}In]In-DO3A-IS1 (Figure S4), comparison of biodistribution among IS-[^{111}In]In-DO2A-ALB1−4 and [^{111}In]In-DO3A-IS1 (Figure S5), biodistribution of IS-[^{111}In]In-DO2A-ALB1−4 and [^{111}In]In-DO3A-IS1 in HT-29 tumor-bearing mice (Tables S2−S6), uptake of IS-[^{111}In]In-DO2A-ALB1 to HT-29 and MDA-MB-231 tumors (Figure S6), biodistribution of IS-[^{111}In]In-IS-DO2A-ALB1 in MDA-MB-231 tumor-bearing mice (Table S7), AUCs for IS-[^{111}In]In-DO2A-ALB1−4 and [^{111}In]In-DO3A-IS1 (Figure S7), AUC values for IS-[^{111}In]In-DO2A-ALB1−4 and [^{111}In]In-DO3A-IS1 in HT-29 tumor-bearing mice (Table S8), SPECT/CT images of HT-29 or MDA-MB-231 tumor-bearing mice with IS-[^{111}In]In-DO2A-ALB1 (Figure S8), maximum intensity projection of SPECT/CT images of an HT-29 tumor-bearing mouse with IS-[^{111}In]In-DO2A-ALB1 (Figure S9), and partition coefficient of IS-[^{111}In]In-DO2A-ALB1−4 and [^{111}In]In-DO3A-IS1 (PDF)

AUTHOR INFORMATION

Corresponding Authors

Shimpei Iikuni − *Department of Patho-Functional Bioanalysis, Graduate School of Pharmaceutical Sciences, Kyoto University, Sakyo-ku, Kyoto 606-8501, Japan;* orcid.org/0000-0002-7073-9084; Phone: +81-75-753-4608; Email: iikuni@pharm.kyoto-u.ac.jp; Fax: +81-75-753-4568

Masahiro Ono − *Department of Patho-Functional Bioanalysis, Graduate School of Pharmaceutical Sciences, Kyoto University, Sakyo-ku, Kyoto 606-8501, Japan;* orcid.org/0000-0002-2497-039X; Phone: +81-75-753-4556; Email: ono@pharm.kyoto-u.ac.jp; Fax: +81-75-753-4568

Authors

Yuya Okada − *Department of Patho-Functional Bioanalysis, Graduate School of Pharmaceutical Sciences, Kyoto University, Sakyo-ku, Kyoto 606-8501, Japan*

Yoichi Shimizu − *Department of Patho-Functional Bioanalysis, Graduate School of Pharmaceutical Sciences, Kyoto University, Sakyo-ku, Kyoto 606-8501, Japan; Department of Diagnostic Imaging and Nuclear Medicine, Kyoto University Graduate School of Medicine, Kyoto University, Sakyo-ku, Kyoto 606-8507, Japan*

Hiroyuki Watanabe − *Department of Patho-Functional Bioanalysis, Graduate School of Pharmaceutical Sciences, Kyoto University, Sakyo-ku, Kyoto 606-8501, Japan;* orcid.org/0000-0002-8873-1224

Complete contact information is available at: https://pubs.acs.org/10.1021/acs.molpharmaceut.0c00953

Author Contributions

[§]S.I. and Y.O. contributed equally to this manuscript.

Notes

The authors declare the following competing financial interest(s): Masahiro Ono received grant support from Nihon Medi-Physics Co., Ltd. The other authors declare no competing financial interests. Masahiro Ono holds a patent related to imidazothiadiazole sulfonamide (IS) derivatives with Nihon Medi-Physics Co., Ltd.

https://dx.doi.org/10.1021/acs.molpharmaceut.0c00953
Mol. Pharmaceutics XXXX, XXX, XXX−XXX

■ ACKNOWLEDGMENTS

Funding: This work was supported, in part, by AMED under Grant JP19im0210819 and Nihon Medi-Physics Co., Ltd.

■ ABBREVIATIONS

ALB, albumin binder; AUC, area under the curve; CA, carbonic anhydrase; CT, computed tomography; DMEM, Dulbecco's modified Eagle's medium; DMF, *N*,*N*-dimethylformamide; EDC, 1-ethyl-3-(dimethylaminopropyl)carbodiimide; ESI, electrospray ionization; FR, folate receptor; HOAt, 1-hydroxybenzotriazole; HRMS, high-resolution mass spectrometry; HSA, human serum albumin; IC_{50}, half-maximal inhibitory concentration; IS, imidazothiadiazole sulfonamide; LC−MS, liquid chromatography−mass spectrometry; MES, 2-(*N*-morpholino)ethanesulfonic acid; NMR, nuclear magnetic resonance; PBS, phosphate-buffered saline; PSMA, prostate-specific membrane antigen; RP-HPLC, reversed-phase high-performance liquid chromatography; SPECT, single-photon emission computed tomography; TFA, trifluoroacetic acid

■ REFERENCES

(1) Supuran, C. T. Carbonic anhydrases: novel therapeutic applications for inhibitors and activators. *Nat. Rev. Drug Discovery* **2008**, *7*, 168−181.

(2) Cosse, J.-P.; Michiels, C. Tumour hypoxia affects the responsiveness of cancer cells to chemotherapy and promotes cancer progression. *Anti-Cancer Agents Med. Chem.* **2008**, *8*, 790−797.

(3) Andreucci, E.; Peppicelli, S.; Carta, F.; Brisotto, G.; Biscontin, E.; Ruzzolini, J.; Bianchini, F.; Biagioni, A.; Supuran, C. T.; Calorini, L. Carbonic anhydrase IX inhibition affects viability of cancer cells adapted to extracellular acidosis. *J. Mol. Med.* **2017**, *95*, 1341−1353.

(4) Yang, J.-S.; Lin, C.-W.; Hsieh, Y.-H.; Chien, M.-H.; Chuang, C.-Y.; Yang, S.-F. Overexpression of carbonic anhydrase IX induces cell motility by activating matrix metalloproteinase-9 in human oral squamous cell carcinoma cells. *Oncotarget* **2017**, *8*, 83088−83099.

(5) Hilvo, M.; Baranauskiene, L.; Salzano, A. M.; Scaloni, A.; Matulis, D.; Innocenti, A.; Scozzafava, A.; Monti, S. M.; Di Fiore, A.; De Simone, G.; Lindfors, M.; Janis, J.; Valjakka, J.; Pastorekova, S.; Pastorek, J.; Kulomaa, M. S.; Nordlund, H. R.; Supuran, C. T.; Parkkila, S. Biochemical characterization of CA IX, one of the most active carbonic anhydrase isozymes. *J. Biol. Chem.* **2008**, *283*, 27799−27809.

(6) Maxwell, P. H.; Wiesener, M. S.; Chang, G.-W.; Clifford, S. C.; Vaux, E. C.; Cockman, M. E.; Wykoff, C. C.; Pugh, C. W.; Maher, E. R.; Ratcliffe, P. J. The tumour suppressor protein VHL targets hypoxia-inducible factors for oxygen-dependent proteolysis. *Nature* **1999**, *399*, 271−275.

(7) Pouysségur, J.; Dayan, F.; Mazure, N. M. Hypoxia signalling in cancer and approaches to enforce tumour regression. *Nature* **2006**, *441*, 437−443.

(8) Ratcliffe, P. J.; Pugh, C. W.; Maxwell, P. H. Targeting tumors through the HIF system. *Nat. Med.* **2000**, *6*, 1315−1316.

(9) Stillebroer, A. B.; Mulders, P. F. A.; Boerman, O. C.; Oyen, W. J. G.; Oosterwijk, E. Carbonic anhydrase IX in renal cell carcinoma: implications for prognosis, diagnosis, and therapy. *Eur. Urol.* **2010**, *58*, 75−83.

(10) Thiry, A.; Dogné, J.-M.; Masereel, B.; Supuran, C. T. Targeting tumor-associated carbonic anhydrase IX in cancer therapy. *Trends Pharmacol. Sci.* **2006**, *27*, 566−573.

(11) Pastorek, J.; Pastorekova, S. Hypoxia-induced carbonic anhydrase IX as a target for cancer therapy: from biology to clinical use. *Semin. Cancer Biol.* **2015**, *31*, 52−64.

(12) Krall, N.; Pretto, F.; Mattarella, M.; Muller, C.; Neri, D. A ^{99m}Tc-labeled ligand of carbonic anhydrase IX selectively targets renal cell carcinoma *in vivo*. *J. Nucl. Med.* **2016**, *57*, 943−949.

(13) Minn, I.; Koo, S. M.; Lee, H. S.; Brummet, M.; Rowe, S. P.; Gorin, M. A.; Sysa-Shah, P.; Lewis, W. D.; Ahn, H.-H.; Wang, Y.; Banerjee, S. R.; Mease, R. C.; Nimmagadda, S.; Allaf, M. E.; Pomper, M. G.; Yang, X. [^{64}Cu]XYIMSR-06: A dual-motif CAIX ligand for PET imaging of clear cell renal cell carcinoma. *Oncotarget* **2016**, *7*, 56471−56479.

(14) Lau, J.; Lin, K.-S.; Bénard, F. Past, present, and future: development of theranostic agents targeting carbonic anhydrase IX. *Theranostics* **2017**, *7*, 4322−4339.

(15) Verhoeff, S. R.; van Es, S. C.; Boon, E.; van Helden, E.; Angus, L.; Elias, S. G.; Oosting, S. F.; Aarntzen, E. H.; Brouwers, A. H.; Kwee, T. C.; Heskamp, S.; Hoekstra, O. S.; Verheul, H.; van der Veldt, A. A. M.; de Vries, E. G. E.; Boerman, O. C.; van der Graaf, W. T. A.; Oyen, W. J. G.; van Herpen, C. M. L. Lesion detection by [^{89}Zr]Zr-DFO-girentuximab and [^{18}F]FDG-PET/CT in patients with newly diagnosed metastatic renal cell carcinoma. *Eur. J. Nucl. Med. Mol. Imaging* **2019**, *46*, 1931−1939.

(16) Iikuni, S.; Okada, Y.; Shimizu, Y.; Watanabe, H.; Ono, M. Synthesis and evaluation of indium-111-labeled imidazothiadiazole sulfonamide derivative for single photon emission computed tomography imaging targeting carbonic anhydrase-IX. *Bioorg. Med. Chem. Lett.* **2020**, *30*, 127255.

(17) Peeters, S. G. J. A.; Dubois, L.; Lieuwes, N. G.; Laan, D.; Mooijer, M.; Schuit, R. C.; Vullo, D.; Supuran, C. T.; Eriksson, J.; Windhorst, A. D.; Lambin, P. [^{18}F]VM4-037 microPET imaging and biodistribution of two *in vivo* CAIX-expressing tumor models. *Mol. Imaging Biol.* **2015**, *17*, 615−619.

(18) Lau, J.; Zhang, Z.; Jenni, S.; Kuo, H.-T.; Liu, Z.; Vullo, D.; Supuran, C. T.; Lin, K.-S.; Bénard, F. PET imaging of carbonic anhydrase IX expression of HT-29 tumor xenograft mice with ^{68}Ga-labeled benzenesulfonamides. *Mol. Pharmaceutics* **2016**, *13*, 1137−1146.

(19) Iikuni, S.; Ono, M.; Watanabe, H.; Shimizu, Y.; Sano, K.; Saji, H. Cancer radiotheranostics targeting carbonic anhydrase-IX with ^{111}In- and ^{90}Y-labeled ureidosulfonamide scaffold for SPECT imaging and radionuclide-based therapy. *Theranostics* **2018**, *8*, 2992−3006.

(20) Nakai, M.; Pan, J.; Lin, K.-S.; Thompson, J. R.; Nocentini, A.; Supuran, C. T.; Nakabayashi, Y.; Storr, T. Evaluation of ^{99m}Tc-sulfonamide and sulfocoumarin derivatives for imaging carbonic anhydrase IX expression. *J. Inorg. Biochem.* **2018**, *185*, 63−70.

(21) Iikuni, S.; Tanimura, K.; Watanabe, H.; Shimizu, Y.; Saji, H.; Ono, M. Development of the ^{99m}Tc-hydroxamamide complex as a probe targeting carbonic anhydrase IX. *Mol. Pharmaceutics* **2019**, *16*, 1489−1497.

(22) Lau, J.; Jacobson, O.; Niu, G.; Lin, K. S.; Bénard, F.; Chen, X. Bench to bedside: albumin binders for improved cancer radioligand therapies. *Bioconjugate Chem.* **2019**, *30*, 487−502.

(23) Dumelin, C. E.; Trüssel, S.; Buller, F.; Trachsel, E.; Bootz, F.; Zhang, Y.; Mannocci, L.; Beck, S. C.; Drumea-Mirancea, M.; Seeliger, M. W.; Baltes, C.; Müggler, T.; Kranz, F.; Rudin, M.; Melkko, S.; Scheuermann, J.; Neri, D. A portable albumin binder from a DNA-encoded chemical library. *Angew. Chem.* **2008**, *47*, 3196−3201.

(24) Chen, H.; Jacobson, O.; Niu, G.; Weiss, I. D.; Kiesewetter, D. O.; Liu, Y.; Ma, Y.; Wu, H.; Chen, X. Novel "add-on" molecule based on Evans blue confers superior pharmacokinetics and transforms drugs to theranostic agents. *J. Nucl. Med.* **2017**, *58*, 590−597.

(25) Fuchigami, T.; Yamashita, Y.; Kawasaki, M.; Ogawa, A.; Haratake, M.; Atarashi, R.; Sano, K.; Nakagaki, T.; Ubagai, K.; Ono, M.; Yoshida, S.; Nishida, N.; Nakayama, M. Characterisation of radioiodinated flavonoid derivatives for SPECT imaging of cerebral prion deposits. *Sci. Rep.* **2016**, *5*, 18440.

(26) Arveschoug, A. K.; Kramer, S. M. J.; Iversen, P.; Frokiaer, J.; Gronbæk, H. Monitoring kidney function in neuroendocrine tumor patients treated with ^{90}Y-DOTATOC: Associations with risk factors. *Curr. Radiopharm.* **2015**, *8*, 49−55.

(27) Baccala, A.; Sercia, L.; Li, J.; Heston, W.; Zhou, M. Expression of prostate-specific membrane antigen in tumor-associated neovasculature of renal neoplasms. *Urology* **2007**, *70*, 385−390.

https://dx.doi.org/10.1021/acs.molpharmaceut.0c00953
Mol. Pharmaceutics XXXX, XXX, XXX−XXX

(28) Kelemen, L. E. The role of folate receptor alpha in cancer development, progression and treatment: cause, consequence or innocent bystander? *Int. J. Cancer* **2006**, *119*, 243−250.
(29) Müller, C.; Struthers, H.; Winiger, C.; Zhernosekov, K.; Schibli, R. DOTA conjugate with an albumin-binding entity enables the first folic acid-targeted ^{177}Lu-radionuclide tumor therapy in mice. *J. Nucl. Med.* **2013**, *54*, 124−131.
(30) Umbricht, C. A.; Benešová, M.; Schibli, R.; Müller, C. Preclinical development of novel PSMA-targeting radioligands: modulation of albumin-binding properties to improve prostate cancer therapy. *Mol. Pharmaceutics* **2018**, *15*, 2297−2306.
(31) Wang, Z.; Jacobson, O.; Tian, R.; Mease, R. C.; Kiesewetter, D. O.; Niu, G.; Pomper, M. G.; Chen, X. Radioligand therapy of prostate cancer with a long-lasting prostate-specific membrane antigen targeting agent ^{90}Y-DOTA-EB-MCG. *Bioconjugate Chem.* **2018**, *29*, 2309−2315.
(32) Kuo, H.-T.; Merkens, H.; Zhang, Z.; Uribe, C. F.; Lau, J.; Zhang, C.; Colpo, N.; Lin, K.-S.; Bénard, F. Enhancing treatment efficacy of ^{177}Lu-PSMA-617 with the conjugation of an albumin-binding motif: preclinical dosimetry and endoradiotherapy studies. *Mol. Pharmaceutics* **2018**, *15*, 5183−5191.
(33) Benešová, M.; Umbricht, C. A.; Schibli, R.; Müller, C. Albumin-binding PSMA ligands: optimization of the tissue distribution profile. *Mol. Pharmaceutics* **2018**, *15*, 934−946.
(34) Kelly, J. M.; Amor-Coarasa, A.; Nikolopoulou, A.; Wüstemann, T.; Barelli, P.; Kim, D.; Williams, C., Jr.; Zheng, X.; Bi, C.; Hu, B.; Warren, J. D.; Hage, D. S.; DiMagno, S. G.; Babich, J. W. Dual-target binding ligands with modulated pharmacokinetics for endoradiotherapy of prostate cancer. *J. Nucl. Med.* **2017**, *58*, 1442−1449.
(35) Dennis, M. S.; Zhang, M.; Meng, Y. G.; Kadkhodayan, M.; Kirchhofer, D.; Combs, D.; Damico, L. A. Albumin binding as a general strategy for improving the pharmacokinetics of proteins. *J. Biol. Chem.* **2002**, *277*, 35035−35043.
(36) Vegt, E.; van Eerd, J. E. M.; Eek, A.; Oyen, W. J. G.; Wetzels, J. F. M.; de Jong, M.; Russel, F. G. M.; Masereeuw, R.; Gotthardt, M.; Boerman, O. C. Reducing renal uptake of radiolabeled peptides using albumin fragments. *J. Nucl. Med.* **2008**, *49*, 1506−1511.

https://dx.doi.org/10.1021/acs.molpharmaceut.0c00953
Mol. Pharmaceutics XXXX, XXX, XXX−XXX